Phonon-Assisted Luminescence in Defect Centers from Many-Body Perturbation Theory

Francesco Libbi,[1,2,*] Pedro Miguel M. C. de Melo,[3,4,5] Zeila Zanolli,[3,5] Matthieu Jean Verstraete,[4,5] and Nicola Marzari[1,2]

[1]*Theory and Simulation of Materials (THEOS), École Polytechnique Fédérale de Lausanne, 1015 Lausanne, Switzerland*
[2]*National Centre for Computational Design and Discovery of Novel Materials (MARVEL), École Polytechnique Fédérale de Lausanne, 1015 Lausanne, Switzerland*
[3]*Chemistry Department, Debye Institute for Nanomaterials Science, Condensed Matter and Interfaces, Utrecht University, PO Box 80.000, 3508 TA Utrecht, Netherlands*
[4]*nanomat/Q-mat/CESAM, Université de Liège, B-4000 Sart Tilman, Liège, Belgium*
[5]*European Theoretical Spectroscopy Facility (ETSF), B-4000 Sart Tilman, Liège, Belgium*

(Received 14 October 2021; revised 18 March 2022; accepted 21 March 2022; published 18 April 2022)

Phonon-assisted luminescence is a key property of defect centers in semiconductors, and can be measured to perform the readout of the information stored in a quantum bit, or to detect temperature variations. The investigation of phonon-assisted luminescence usually employs phenomenological models, such as that of Huang and Rhys, with restrictive assumptions that can fail to be predictive. In this work, we predict luminescence and study exciton-phonon couplings within a rigorous many-body perturbation theory framework, an analysis that has never been performed for defect centers. In particular, we study the optical emission of the negatively charged boron vacancy in 2D hexagonal boron nitride, which currently stands out among defect centers in 2D materials thanks to its promise for applications in quantum information and quantum sensing. We show that phonons are responsible for the observed luminescence, which otherwise would be dark due to symmetry. We also show that the symmetry breaking induced by the static Jahn-Teller effect is not able to describe the presence of the experimentally observed peak at 1.5 eV.

DOI: 10.1103/PhysRevLett.128.167401

In the last decade defect centers in semiconductors have been increasingly studied for their applications in quantum computing [1], quantum communication [2,3], and quantum sensing [4–8]. Quantum information is usually stored in a paramagnetic ground state, which is manipulated through electromagnetic radiation, often in the range of microwaves. Optical properties of the defect centers play a major role in quantum information and quantum sensing: spin-dependent luminescence can be used to perform the readout [9,10] of defect centers which are responsive to optically detected magnetic resonance (ODMR), allowing these systems to be used as practical qubits. Furthermore, the sharp temperature dependence of the peaks of the photoluminescence (PL) spectrum can be used to design sensitive thermometers [11].

In the last years, a great deal of attention has been focused on defect centers in 2D hexagonal boron nitride [12–15], where a wide band gap, together with low spin-orbit coupling and reduced dimensionality, may overcome the limitations of existing 3D defect centers in terms of coherence [16], resolution and interfaceability with cavities and resonators [17]. In particular, the negatively charged boron vacancy (V_B^-) in 2D hBN has been predicted to be responsive to ODMR (and thus usable for quantum computing), and to emit in the infrared when stimulated with continuous green laser light [17].

Because of the coupling of excitons with vibronic modes of the atoms around a defect, the photoluminescence of defect centers in semiconductors is often phonon assisted. This is usually studied using the Huang-Rhys model [18–23], whose parameters are determined through constrained-DFT or quantum-chemistry calculations, as reviewed in Ref. [24]. The Huang-Rhys model, however, is based on restrictive hypotheses (summarized in the Supplemental Material [25]), such as the assumption that the optical dipole moments are not affected by phonons, which limit its predictive power. Furthermore, it does not lead to an interpretation of the phonon-assisted luminescence in terms of coupling between excitons and phonons, which is essential for the understanding of this phenomenon.

The optical properties of *pristine* hBN have been studied using many-body perturbation theory (MBPT) [35,36], and its phonon-assisted emission spectrum has been calculated both for the bulk and the monolayer [37–39]. However, due to the complexity and computational cost of these analyses, the luminescence of defect centers has never been studied with such advanced methods.

In the following, we investigate the optical properties of the negatively charged boron vacancy in 2D hBN using first-principles many-body perturbation theory, and compare with the experimental results of Ref. [24]. This predictive approach for the luminescence of defect centers

gives a universal tool to include the nontrivial couplings beyond the Huang-Rhys theory for PL line shapes, and allows us to reach an unprecedented microscopic understanding of the emission mechanism in these systems. In particular, we study the coupling between excitons and phonons leading to the phonon-assisted luminescence, and identify the phonon modes which interact most strongly with excitons, thus leading to peaks in the sideband of the emission spectrum. We show that the phonon-independent emission is dark due to symmetry reasons, and prove that the emission observed experimentally is due to the symmetry breaking caused by phonons. Conversely, we show that the symmetry breaking induced by the static Jahn-Teller effect is not able to activate photoluminescence. The remarkable agreement between theoretical and experimental PL, together with the lack of *ad hoc* parameters underscore the predictive accuracy of such approach.

In a photoluminescence measurement, the system is excited with a laser beam, leading to the formation of excitons. These undergo a series of scattering processes, mainly with phonons and other excitons, as a consequence of which electrons and holes relax respectively towards the bottom of the conduction band and the top of the valence band, before the radiative or nonradiative recombination takes place, with the emission of photons and/or phonons [40,41]. If the excited state dynamics continues for long enough, it is reasonable to assume that both electron and holes thermalise, with pseudoequilibrium occupations equal to

$$f_{n\mathbf{k}} = \frac{1}{e^{\frac{\varepsilon_{n\mathbf{k}}-\mu_{el}}{k_B T}}+1}, \quad \bar{f}_{n\mathbf{k}} = \frac{1}{e^{-\frac{\varepsilon_{n\mathbf{k}}-\mu_{ho}}{k_B T}}+1} \tag{1}$$

for electrons and holes, respectively. Here $\varepsilon_{n\mathbf{k}}$ is the quasiparticle energy of the state $\{n\mathbf{k}\}$ and μ_{el} (μ_{ho}) the chemical potential for electrons (holes). The values for μ_{el} and μ_{ho}, as well as the parameters used in the simulations, are reported in the Supplemental Material [25].

To proceed, we first determine the absorption spectrum by solving the equilibrium Bethe-Saltpeter equation (BSE) for the two-particle correlation function, as reported in the Supplemental Material [25]. Then, we calculate the photoluminescent emission by solving the nonequilibrium BSE for the electron-electron correlation function, following the approach of Ref. [37]. The coupling with phonons as a function of laser frequency ω and temperature T is included in the simulations via:

$$I_{\mathrm{ph}}(\omega,T) \propto \sum_{\lambda,\nu} \frac{\partial^2|\Pi_\lambda|^2}{\partial x_\nu^2} f_\lambda^< \left[\delta(\omega - E_\lambda - \omega_\nu)\frac{n_B(\omega_\nu,T)}{2\omega_\nu} + \delta(\omega - E_\lambda + \omega_\nu)\frac{1+n_B(\omega_\nu,T)}{2\omega_\nu}\right], \tag{2}$$

with exciton mode λ of energy E_λ changing with respect to the displacement x_ν induced by a phonon ν of frequency ω_ν. The second derivative of the dipole moment Π_λ gauges the intensity of the coupling between the exciton and the phonon. Here, $f_\lambda^<$ is the non-equilibrium exciton occupation function, which is nonvanishing only if the excitons are composed by transitions between bands occupied by excited electrons and holes, and the two Dirac δ in the square bracket correspond to the cases where an exciton recombines with the creation $[\delta(\omega - E_\lambda + \omega_\nu)]$ or annihilation $[\delta(\omega - E_\lambda - \omega_\nu)]$ of a phonon; n_B is the Bose-Einstein occupation function for phonon ν at temperature T. Equation (2) represents a first order effect, the zero order being the phonon-independent photoluminescence expression:

$$I_0 = \sum_\lambda |\Pi_\lambda^2| f_\lambda^< \delta(\omega - E_\lambda). \tag{3}$$

However, as it will be shown later, the phonon-independent luminescence of this system is extremely weak; therefore, it can be neglected and only the first-order term due to phonons survives. Figure 1 compares the theoretically predicted photoluminescence and the experimental one at 300 K, showing very good agreement both for the position of the peak and the shape of the spectrum; the inset of Fig. 1 shows the theoretical and experimental spectra after aligning the zero phonon lines (ZPLs). The experimental ZPL, 1.64 eV at $T = 295$ K, is taken from the supplemental material of Ref. [24]. The theoretical ZPL is assumed to coincide with the energy of the exciton contributing the most to the photoluminescence spectrum (this choice is discussed in detail later). In order to identify the contribution of each exciton to the photoluminescence spectrum it is useful to plot a simplified version of Eq. (2):

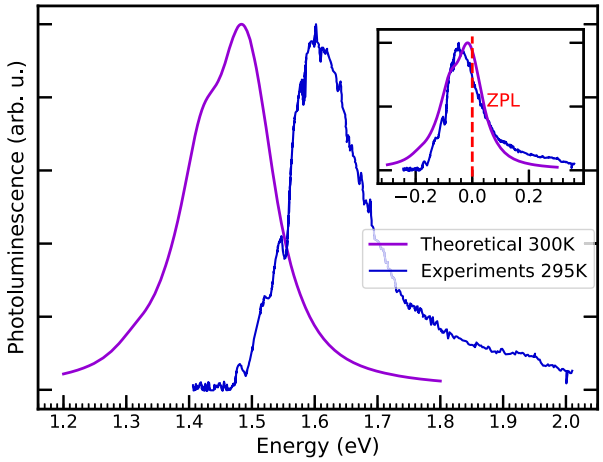

FIG. 1. Theoretically predicted phonon-assisted luminescence [Eq. (2)], normalized and compared to experiments [24], at $T = 300$ K. The insets shows the theoretical and experimental curves after aligning the ZPLs.

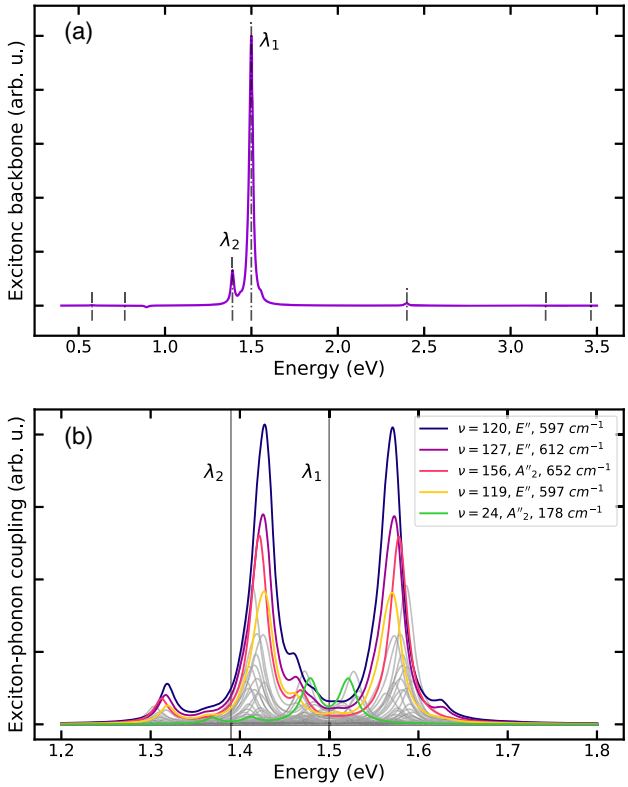

FIG. 2. Panel (a) shows the exciton backbone, as defined in Eq. (4) and normalized. It is clearly dominated by a main excitonic peak at 1.50 eV (λ_1), which is assumed to coincide with the ZPL of the system, while a smaller detached peak appears at 1.39 eV (λ_2). Panel (b) represents instead the exciton phonon coupling function, as defined in Eq. (5). The phonon modes which couple most strongly with excitons are enlightened with colored lines and reported in the legend in decreasing order of contribution, while the other phonon modes are represented with gray lines. Mode $\nu = 24$ is not among those coupling most strongly with excitons; however its contribution to the PL will become one of the highest when including the Bose-Einstein terms, as shown in the Supplemental Material [25].

$$B(\omega) = \sum_{\lambda,\nu} \frac{\partial^2 |\Pi_\lambda|^2}{\partial x_\nu^2} f_\lambda^< \delta(\omega - E_\lambda), \tag{4}$$

which is obtained by replacing the Dirac δ corresponding to the phonon absorption and emission with a single Dirac δ centered at the exciton energy. This simplified expression has the merit of highlighting the "excitonic backbone" which stands behind the spectra of Fig. 1. As shown in Fig. 2(a) this backbone is dominated by a main peak at 1.5 eV (λ_1) and a smaller peak at 1.39 eV (λ_2). The peak at 1.5 eV is distributed into multiple new ones by phonons, whose sum leads to the main peaks of the curve reported in Fig. 1. The peak at 1.39 eV in the exciton backbone is instead responsible for the shoulder that appears in the spectra of Fig. 1 towards 1.3 eV. The experimental spectrum is asymmetric with a shoulder at low energy which may correspond to the 1.3 eV peak, though the intensity ratio is different. If the phonons had vanishing frequency, almost all the emission would take place at 1.5 eV, which is the energy of the bare exciton contributing most to the photoluminescence spectrum. Taking this as a definition of the "zero phonon line" then 1.5 eV can be used for a direct comparison with the ZPL of the Huang-Rhys model. The error of 0.14 eV between the experimental (1.64 eV) and theoretical (1.5 eV) ZPLs witness a very good agreement between simulations and experiments.

In order to understand which phonon modes couple most strongly with excitons, we plot a simplified version of Eq. (2), defining the "exciton-phonon coupling" function

$$C(\omega) = \sum_{\lambda,\nu} \frac{\partial^2 |\Pi_\lambda|^2}{\partial x_\nu^2} f_\lambda^< [\delta(\omega - E_\lambda - \omega_\nu) + \delta(\omega - E_\lambda + \omega_\nu)] \tag{5}$$

obtained from Eq. (2) by removing the Bose-Einstein distributions, which otherwise would affect the amplitudes of the peaks and would depend on temperature. We can see from Fig. 2(b) that the mode that couples most with excitons is $\nu = 120$, of frequency 597 cm^{-1} and symmetry E'', which is characterized by an out-of-plane oscillation of the first and second nearest neighbours around the vacancy (as shown in the Supplemental Material [25]). The other phonon modes which dominate the exciton-phonon coupling function have similar frequencies to mode $\nu = 120$ and either E'' or A_2'' symmetry (mode $\nu = 24$, characterized by in-phase out-of-plane oscillation of the nitrogen atoms around the vacancy). This ranking is overturned by the Bose-Einstein occupations, especially at high temperatures. As discussed in detail in the Supplemental Material [25], the effects of the terms $\{[n_B(\omega, T) + 1]/2\omega\}$ and $[n_B(\omega, T)/2\omega]$ are (i) to increase the contribution to PL of the low energy phonons at high temperatures, (ii) to suppress the contribution of the phonon annihilation term at low temperatures.

Chen *et al.* [11] suggest to use defects in 2D hBN as sensitive local thermometers, by exploiting the temperature dependence of the full-width at half-maximum (FWHM) of the PL. We calculate the FWHM for a set of temperatures ranging from 0 to 600 K (Fig. 3) and observe an initial very steep increase, due to the combined effects of the increasing contribution of the phonon annihilation term and the increasing importance of lower energy modes. Eventually the low frequency (178 cm^{-1}) phonon mode $\nu = 24$ of symmetry A_2'' starts to dominate the PL spectrum. Lower ω lead to smaller energy splittings, and beyond 200 K our exciton-phonon coupling model predicts a smooth decrease in the FWHM, but we emphasize that we are neglecting anharmonic phonon lifetimes as well as multiphonon effects beyond the perturbation theory used here. These would add to the full spectral peak width,

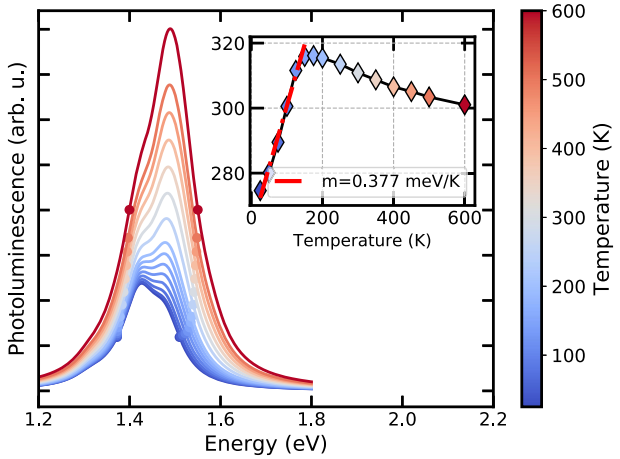

FIG. 3. Temperature dependence of the phonon-assisted luminescence spectrum. The pair of dots that are plotted for each spectrum show the points where it has a value which is half its maximum. The inset shows the behavior of this FWHM (in meV) as a function of temperature. Note that the increase of the curves along the vertical axis is not quantitative, as Eq. (2) does not fix the amplitude of the PL spectrum: only the shape and width are relevant.

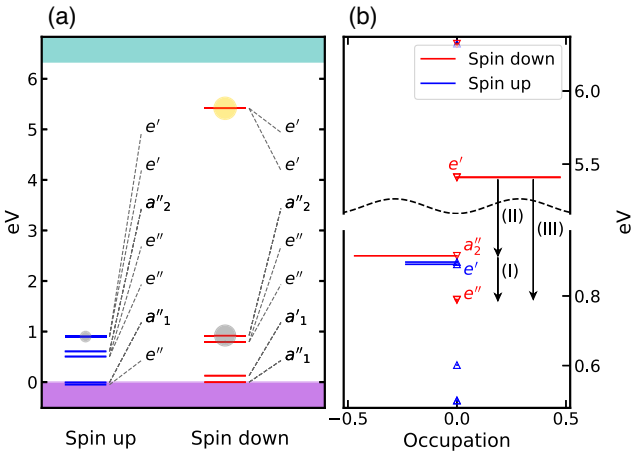

FIG. 4. Panel (a) shows the defect levels inside the band-gap for V_B^- center in 2D hBN, determined through G_0W_0 calculations. The blue and red lines represent spin-up and spin-down levels, respectively. The yellow and gray circles represent pictorially the nonequilibrium occupations of the levels. Panel (b) shows the nonequilibrium occupations of the defect levels as a function of their nonrenormalized energies. The black arrows mark the only possible recombinations which can give rise to photoluminescence.

but are of very different nature. A linear fit of the FWHM from 0 to 200 K yields a coefficient of 0.343 meV/K, which shows very high sensitivity to temperature variations and suggests that this defect can indeed be used as a nanoscale thermometer.

In the final part of this work we argue that mechanisms other than phonon dressing cannot explain the observed photoluminescence. We calculate first the phonon-independent luminescence from Eq. (3), and interpret it by studying the defect levels involved, and their nonequilibrium occupations. The negatively charged boron vacancy generates many donor states close to the valence band, but just one doubly degenerate spin-down acceptor close to the conduction band [Fig. 4(a)]. The presence of this acceptor opens the spin-down transition channels inside the band gap, which will be responsible for the observed photoluminescence, as discussed later. In Fig. 4(b) we show the nonequilibrium occupation of the defect levels [Eq. (1)] as a function of their quasiparticle energy at 300 K. Only the energy levels closest to the middle of the band gap will show significant populations (with a thermal width of 26 meV). The spin down degenerate levels e' are occupied on average by one excited electron (0.5 each), while the spin down a_2'' level by close to 0.5 holes. The spin down level e'' has a very small but not negligible population (0.006 holes), while all the other spin down levels are empty.

The phonon-independent photoluminescence spectrum reported in Fig. 5 is made up of three main peaks: the first peak at 0.6 eV (I in Fig. 5) is mainly associated to the spin down $a_2'' \rightarrow e''$ transition, which has a non vanishing in-plane dipole. Because of the very small hole population of the level e'', this peak is expected to be extremely weak, and is not observed in experiments; for the same reason the third peak at 3.3 eV (III in Fig. 5) is very weak and not observed, despite the finite out-of-plane dipole moment of the transition. It is associated to the transition between the spin down levels e' and e''. Last, the second peak at 1.5 eV (II in Fig. 5) is associated to the transition from the spin down level e' to a_2'', which is the only one where both the levels involved have a non-negligible population in terms

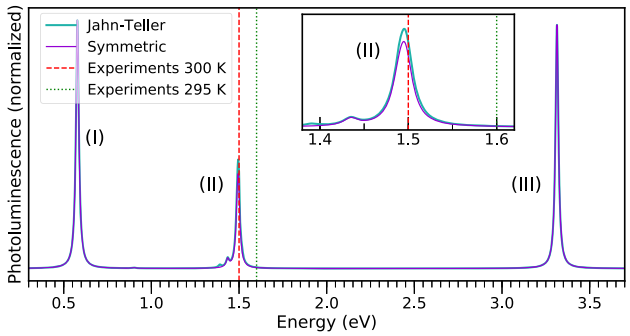

FIG. 5. The phonon-independent photoluminescence spectrum of the original symmetric system (purple solid line) is compared to that of the Jahn-Teller distorted system (light blue solid line). The roman numbers indicate which of the recombinations reported in Fig. 4(b) is associated to the peak. The activation of the transition $a_1 \rightarrow b_2$ caused by the symmetry breaking due to the Jahn-Teller effect leads to an enhancement of the peak at 1.5 eV, which, however, is still weaker than the other two peaks and therefore not observable by experiments.

of electrons or holes. However, this transition is prohibited by symmetry, therefore the corresponding peak is even weaker than the others. It is important to stress that the creation of this exciton from the transition $e' \to a_2''$ is achieved thanks to nonequilibrium occupations: there is no trace of an exciton at 1.5 eV with the same composition when solving the equilibrium BSE. So, two of the three peaks are very weak because of population arguments, and are not observed in experiments, while a third peak, which has the same energy of the peak observed experimentally (1.5 eV), is dark due to symmetry reasons. Following this analysis, we can conclude that there must be some symmetry-breaking phenomenon which enables the transition $e' \to a_2''$ (the only one which is not removed by the lack of electron or hole population) and leads to the peak at 1.5 eV which dominates the photoluminescence spectrum, and makes it observable by experiments. The two main candidate mechanisms to activate the second peak are the Jahn-Teller distortion of the excited state e', and lattice vibrations.

We have seen above in Fig. 2(a) that the symmetry reduction associated with lattice vibrations allows the transition $e' \to a_2''$, thus leading to the peak at 1.5 eV to dominate the exciton backbone spectrum. We now show that the static Jahn-Teller effect, instead, is not enough to activate the second peak. The doubly degenerate excited state which is obtained promoting an electron from a_2'' to e' can undergo a Jahn-Teller distortion which reduces the symmetry of the system from D_{3h} to C_{2v}, splits the level e' into a_1 and b_1, and changes the irreducible representation of the level a_2'' into b_2 (see Fig. 8 in the Supplemental Material [25]). The transition $a_1 \to b_2$ has now a nonvanishing out of-plane-dipole, while the transition $b_1 \to b_2$ is still forbidden. We calculate the luminescence for the Jahn-Teller distorted system. As shown in Fig. 5, the activation of the transition $a_1 \to b_2$ caused by the symmetry break leads to an enhancement of the peak at 1.5 eV. This enhancement, however, is still not sufficient, as this peak remains weaker than the other two peaks, which are not observable as discussed before. Therefore, we conclude that the static Jahn-Teller effect is not the symmetry breaking phenomenon which activates the photoluminescence and the peak observed at 1.5 eV. A tell tale signature for this reasoning can be also found in the lack of an apparent ZPL in the experimental spectra.

In conclusion, we studied the phonon-assisted luminescence of the negatively charged boron vacancy in 2D hBN using MBPT. Our simulations show that the phonon-independent luminescence is extremely weak, even when the static Jahn-Teller effect is included. Instead, phonons of E'' and A_2'' symmetry are responsible for the observed luminescence. At low temperatures, the luminescence is determined by high frequency modes which are strongly coupled with excitons. At $T > 200$ K the PL spectrum becomes dominated by low-frequency modes due to the Bose-Einstein statistics. The temperature dependence of the FWHM shows a very sensitive behaviour of the PL spectrum with the temperature, suggesting that this defect can be used as a nanoscale thermometer, at least in a range of temperatures between 0 and 200 K. The agreement between theory and experiments is very good, and we hope our explanation of the photoluminescence mechanisms will further the technological integration of defect centers for quantum information and sensing.

This project has received funding from the European Union's Horizon 2020 research and innovation program under the Marie Sklodowska-Curie Grant Agreement No. 754354 and was supported by the NCCR MARVEL, a National Centre of Competence in Research, funded by the Swiss National Science Foundation (Grant No. 182892), and H2020 MaX Centre of Excellence on "Materials design at the Exascale," Grant Agreement No. 824143. M. J. V. and P. M. M. C. were funded by the Fonds de la Recherche Scientifique (FRS-FNRS Belgium) through PdR Grant No. T.0103.19—ALPS. Simulation time was awarded by PRACE on Marconi at Cineca, Italy (Project No. 2016163963) and by PRACE optospin on Mare Nostrum at Barcelona Supercomputing center, Spain (Project No. 2020225411). Z. Z. and P. M. M. C. acknowledge financial support by the Netherlands Sector Plan program 2019-2023. M. J. V. acknowledges funding from Federation Wallonie Bruxelles through Actions de Recherches Concertées project DREAMS g.a. ARC 21/25-11.

*francesco.libbi@epfl.ch

[1] L. Childress, M. V. Gurudev Dutt, J. M. Taylor, A. S. Zibrov, F. Jelezko, J. Wrachtrup, P. R. Hemmer, and M. D. Lukin, Science **314**, 281 (2006).
[2] W. Pfaff, B. J. Hensen, H. Bernien, S. B. van Dam, M. S. Blok, T. H. Taminiau, M. J. Tiggelman, R. N. Schouten, M. Markham, D. J. Twitchen, and R. Hanson, Science **345**, 532 (2014).
[3] L. Childress, J. M. Taylor, A. S. Sørensen, and M. D. Lukin, Phys. Rev. Lett. **96**, 070504 (2006).
[4] L. T. Hall, J. H. Cole, C. D. Hill, and L. C. L. Hollenberg, Phys. Rev. Lett. **103**, 220802 (2009).
[5] G. de Lange, D. Ristè, V. V. Dobrovitski, and R. Hanson, Phys. Rev. Lett. **106**, 080802 (2011).
[6] F. Dolde, M. W. Doherty, J. Michl, I. Jakobi, B. Naydenov, S. Pezzagna, J. Meijer, P. Neumann, F. Jelezko, N. B. Manson, and J. Wrachtrup, Phys. Rev. Lett. **112**, 097603 (2014).
[7] M. W. Doherty, V. V. Struzhkin, D. A. Simpson, L. P. McGuinness, Y. Meng, A. Stacey, T. J. Karle, R. J. Hemley, N. B. Manson, L. C. L. Hollenberg, and S. Prawer, Phys. Rev. Lett. **112**, 047601 (2014).
[8] P. Neumann, I. Jakobi, F. Dolde, C. Burk, R. Reuter, G. Waldherr, J. Honert, T. Wolf, A. Brunner, J. H. Shim, D. Suter, H. Sumiya, J. Isoya, and J. Wrachtrup, Nano Lett. **13**, 2738 (2013).

[9] D. M. Toyli, C. F. de las Casas, D. J. Christle, V. V. Dobrovitski, and D. D. Awschalom, Proc. Natl. Acad. Sci. U.S.A. **110**, 8417 (2013).
[10] M. Steiner, P. Neumann, J. Beck, F. Jelezko, and J. Wrachtrup, Phys. Rev. B **81**, 035205 (2010).
[11] Y. Chen, T. N. Tran, N. M. H. Duong, C. Li, M. Toth, C. Bradac, I. Aharonovich, A. Solntsev, and T. T. Tran, ACS Appl. Mater. Interfaces **12**, 25464 (2020).
[12] M. Kianinia, S. White, J. E. Fröch, C. Bradac, and I. Aharonovich, ACS Photonics **7**, 2147 (2020).
[13] N. Mendelson, D. Chugh, J. R. Reimers, T. S. Cheng, A. Gottscholl, H. Long, C. J. Mellor, A. Zettl, V. Dyakonov, P. H. Beton, S. V. Novikov, C. Jagadish, H. H. Tan, M. J. Ford, M. Toth, C. Bradac, and I. Aharonovich, Nat. Mater. **20**, 321 (2021).
[14] R. Bourrellier, S. Meuret, A. Tararan, O. Stéphan, M. Kociak, L. H. G. Tizei, and A. Zobelli, Nano Lett. **16**, 4317 (2016).
[15] L. Museur, E. Feldbach, and A. Kanaev, Phys. Rev. B **78**, 155204 (2008).
[16] M. Ye, H. Seo, and G. Galli, npj Comput. Mater. **5**, 44 (2019).
[17] A. Gottscholl, M. Kianinia, V. Soltamov, S. Orlinskii, G. Mamin, C. Bradac, C. Kasper, K. Krambrock, A. Sperlich, M. Toth, I. Aharonovich, and V. Dyakonov, Nat. Mater. **19**, 540 (2020).
[18] K. Huang and A. Rhys, Proc. R. Soc. A **204**, 406 (1950).
[19] A. Alkauskas, B. B. Buckley, D. D. Awschalom, and C. G. V. de Walle, New J. Phys. **16**, 073026 (2014).
[20] V. Ivády, G. Barcza, G. Thiering, S. Li, H. Hamdi, J.-P. Chou, Ö. Legeza, and A. Gali, npj Comput. Mater. **6**, 41 (2020).
[21] Y. Jin, M. Govoni, G. Wolfowicz, S. E. Sullivan, F. J. Heremans, D. D. Awschalom, and G. Galli, Phys. Rev. Mater. **5**, 084603 (2021).
[22] T. H. Keil, Phys. Rev. **140**, A601 (1965).
[23] M. Lax, J. Chem. Phys. **20**, 1752 (1952).
[24] J. R. Reimers, J. Shen, M. Kianinia, C. Bradac, I. Aharonovich, M. J. Ford, and P. Piecuch, Phys. Rev. B **102**, 144105 (2020).
[25] See Supplemental Material at http://link.aps.org/supplemental/10.1103/PhysRevLett.128.167401 for details concerning the parameters adopted in the simulations, the absorption spectrum, the phonon calculation, the effect of nonequilibrium occupations and the comparison with the Huang-Rhys model, which includes Refs. [26–34].
[26] P. Giannozzi *et al.*, J. Phys. Condens. Matter **21**, 395502 (2009).
[27] M. van Setten, M. Giantomassi, E. Bousquet, M. Verstraete, D. Hamann, X. Gonze, and G.-M. Rignanese, Comput. Phys. Commun. **226**, 39 (2018).
[28] A. Marini, C. Hogan, M. Grüning, and D. Varsano, Comput. Phys. Commun. **180**, 1392 (2009).
[29] D. Sangalli, A. Ferretti, H. Miranda, C. Attaccalite, I. Marri, E. Cannuccia, P. Melo, M. Marsili, F. Paleari, A. Marrazzo, G. Prandini, P. Bonfà, M. O. Atambo, F. Affinito, M. Palummo, A. Molina-Sánchez, C. Hogan, M. Grüning, D. Varsano, and A. Marini, J. Phys. Condens. Matter **31**, 325902 (2019).
[30] A. Togo and I. Tanaka, Scr. Mater. **108**, 1 (2015).
[31] C. Attaccalite, M. Bockstedte, A. Marini, A. Rubio, and L. Wirtz, Phys. Rev. B **83**, 144115 (2011).
[32] M. Tinkham, *Group Theory and Quantum Mechanics* (Dover Publications, New York, 2003).
[33] T. T. Tran, C. Zachreson, A. M. Berhane, K. Bray, R. G. Sandstrom, L. H. Li, T. Taniguchi, K. Watanabe, I. Aharonovich, and M. Toth, Phys. Rev. Applied **5**, 034005 (2016).
[34] T. Sohier, M. Gibertini, M. Calandra, F. Mauri, and N. Marzari, Nano Lett. **17**, 3758 (2017).
[35] L. Sponza, H. Amara, F. Ducastelle, A. Loiseau, and C. Attaccalite, Phys. Rev. B **97**, 075121 (2018).
[36] L. Sponza, H. Amara, C. Attaccalite, S. Latil, T. Galvani, F. Paleari, L. Wirtz, and F. Ducastelle, Phys. Rev. B **98**, 125206 (2018).
[37] E. Cannuccia, B. Monserrat, and C. Attaccalite, Phys. Rev. B **99**, 081109(R) (2019).
[38] F. Paleari, H. P. C. Miranda, A. Molina-Sánchez, and L. Wirtz, Phys. Rev. Lett. **122**, 187401 (2019).
[39] L. Schué, L. Sponza, A. Plaud, H. Bensalah, K. Watanabe, T. Taniguchi, F. Ducastelle, A. Loiseau, and J. Barjon, Phys. Rev. Lett. **122**, 067401 (2019).
[40] E. Perfetto, D. Sangalli, A. Marini, and G. Stefanucci, Phys. Rev. B **92**, 205304 (2015).
[41] P. M. M. C. de Melo and A. Marini, Phys. Rev. B **93**, 155102 (2016).